Improving Scour Estimates with NextScour for the Lafayette Avenue Bridge Replacement Project

Haoyin Shan, *Research Hydraulic Engineer, Genex Systems, McLean, VA, USA; email:* haoyin.shan.ctr@dot.gov
James Pagenkopf, *Research Hydraulic Engineer, Federal Highway Administration, McLean, VA; email:* james.pagenkopf@dot.gov
Chen Li, *Research Hydraulic Engineer, Genex Systems, McLean, VA, USA; email:* chen.li.ctr@dot.gov
Nasi Zhang, *Research Hydraulic Engineer, Genex Systems, McLean, VA, USA; email:* nasi.zhang.ctr@dot.gov
Daniel Pastrich, *Research Engineer, McLean, VA, USA; email:* danielpastrich@gmx.de
Otto Wiblishauser, *Research Engineer, Genex Systems, McLean, VA, USA; email:* o.wiblishauser.ctr@dot.gov
Chao Huang, *Research Hydraulic Engineer, Genex Systems, McLean, VA, USA; email:* c.huang.ctr@dot.gov
Kornel Kerenyi, *Research Hydraulic Engineer, Federal Highway Administration, McLean, VA, USA; email:* kornel.kerenyi@dot.gov

ABSTRACT: *The Michigan Department of Transportation (MDOT) is investigating replacing the existing Lafayette Avenue Bridge in Bay City, MI. The geotechnical site investigation classified a layer of medium-to-hard clay at depths of 4.6 to 6.1 m (15–20 ft) below the channel that potentially and significantly reduces scour and makes the foundation design more economical. Conventional design methods predict scour depths that would penetrate the clay layer by several feet. MDOT reached out to the Federal Highway Administration (FHWA) through the Transportation Pooled Fund Program for help in applying the latest advancements in scour research for this project. FHWA suggested using the NextScour method to conduct the scour analysis. NextScour recognizes that the phenomenon of scour consists of two major aspects or components: consideration of water and hydraulic forces (loads), and the erosion resistance of soils and their associated geotechnical effects (resistance). NextScour institutes a new direction; it refocuses and aligns those geotechnical and hydraulic components within a true multidisciplinary framework, with outcomes that provide more certainty and reduced project costs. This paper summarizes how the NextScour approach helps improve the design scour determination for the Lafayette Avenue Bridge replacement project.*

KEYWORDS: NextScour, clay, erosion resistance, critical shear stress, erosion testing, decay function.

SITE LOCATION: **Geo-Database**

INTRODUCTION

Project Background

The Lafayette Avenue Bridge carries state routes M-13/M-84 over the east channel of the Saginaw River on the south side of Bay City, MI. The west abutment rests on Middle Ground Island, and a second fixed bridge connects to Salzburg Avenue over the narrower west channel of the river. Originally opened in 1938, the Lafayette Avenue Bridge features two bascule piers that support a 56.4-m (185-ft)-long bascule span, which frequently opens for commercial and recreational vessels. It has a 9.1-m (30-ft) roadway width between curbs and carries one traffic lane in each direction. In addition, there are 1.5-m (5-ft)-wide sidewalks on both sides of the roadway. The bridge comprises a double leaf rolling lift bascule span flanked on both ends by single steel plate girder approach spans. The bridge has substructures supported by deep timber pile foundations. Over the years, the substructures have had concrete patching and crack-sealing repairs during previous rehabilitations, with their primary structural reinforced concrete elements remaining from the original construction (URS, 2014).

The bridge was rehabilitated in 1987 to replace the bascule and approach span superstructures, but the existing substructure was retained. Since its replacement, the bascule span has exhibited severe problems with the curved steel tread plates (URS, 2014). These problems have resulted in numerous repair efforts and require frequent attention. The bridge is scour critical (NBI, 2021). As part of the 1988 rehabilitation, scour countermeasures were installed to address areas where scour had undermined and exposed the supporting timber piles at the upstream end of both bascule piers. A URS report for the Michigan Department of Transportation (MDOT) indicated that a 2013 hydrographic survey after high-water conditions identified two new, large scour holes on the downstream side of the bascule span without the actual scour depths (URS, 2014). Based on a 90-year life and including both the estimated cost of an initial construction project and costs for future project needs, URS (2014) concluded that "life cycle cost analysis computations indicate that the bridge replacement alternative would also have a greater net present value."

The new bridge that MDOT has proposed, shown in Figure 1, will replace the entire substructure and superstructure in the current location of the existing bridge. The total length would increase from 138.9 m (456 ft) to 156.4 m (513 ft). The proposed piers are larger than the current piers and are farther apart to maintain a bascule span distance of 57.9 m (190 ft). The proposed left and right abutments are set farther back than the current ones to provide additional relief to the main channel. The proposed left abutment is spill through, whereas the right abutment is a vertical wall abutment carrying a pedestrian path under the approach span. The proposed foundations feature H-pile (HP) supports for all piers and abutments. In addition, MDOT plans to install cofferdams around each pier's perimeter to protect the piles.
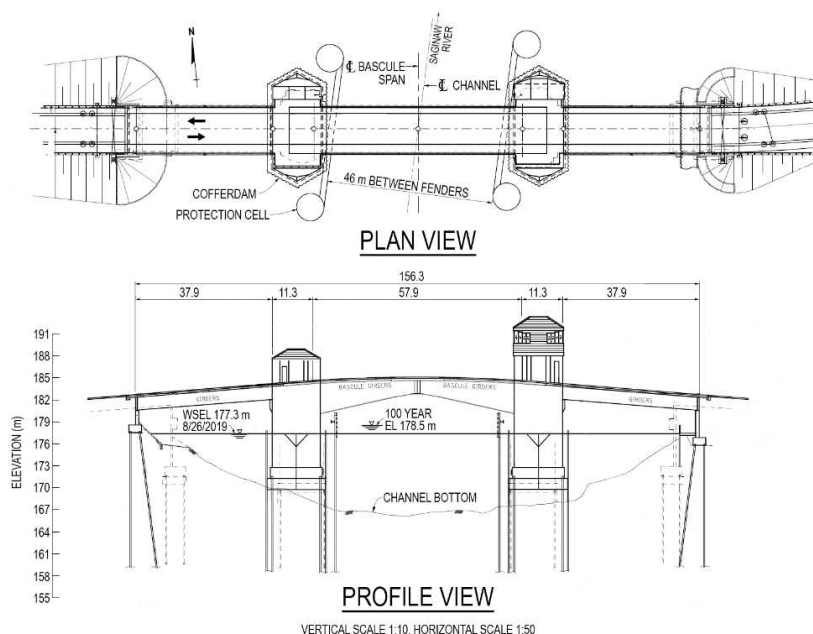

Figure 1. Plan and profile views of the proposed Lafayette Avenue Bridge, © 2020 MDOT. Modifications by FHWA.

MDOT plans to install a fender system with a 46-m (151-ft) clearance between the piers to protect the bascule piers from passing vessels. Each fender features a 7.6-m (25-ft)-diameter cell up- and downstream of the piers. The fender plates align with the river at a slight 7.5-degree skew with the bridge.

Subsurface Soil Profile and Geotechnical Properties

The subsurface soil profile at the site was determined from a 2016 geotechnical site investigation. Five soil borings were completed in the floodplain surrounding each abutment. Two additional borings in the channel were upstream and downstream of each pier. The investigation revealed that the subsurface soils at both overbanks had an initial layer of fill consisting of loose sand and silt, followed by a layer of decomposed wood, sawdust, sand, and silt, with traces of gravel. The right overbank then transitioned to a 4.6-m- (15-ft) thick layer of poorly graded sand. The left overbank (part of Middle Ground Island) was found to have silt and sand layers at this level. From an elevation of 168.6 m (553 ft) in the right overbank and 162.5 m (533 ft) in the left overbank, the soil profile transitioned to a thick layer of stiff, gray, lean clay that continued down to an elevation of 147.8 m (485 ft), where it reached a layer of shale.

The main channel bed featured a thin layer of river sediment, which consisted of clayey/sandy silt. The corresponding median particle diameter (D_{50}) of this fine, silty sand was found to be 0.1 mm (0.004 in). Beneath that was a layer of poorly graded, loose sand and silty sand that varied in thickness between 1.5 and 3.0 m (5 and 10 ft). Between 162.5 and 164.6 m (533 and 540 ft), the sand layer transitioned to the thick layer of lean clay across the overbanks. The borings suggested that this clay layer was continuous across the entire profile of the channel. A generalized subsurface profile at the centerline of the existing bridge was created by using the boring data and is shown in Figure 2.
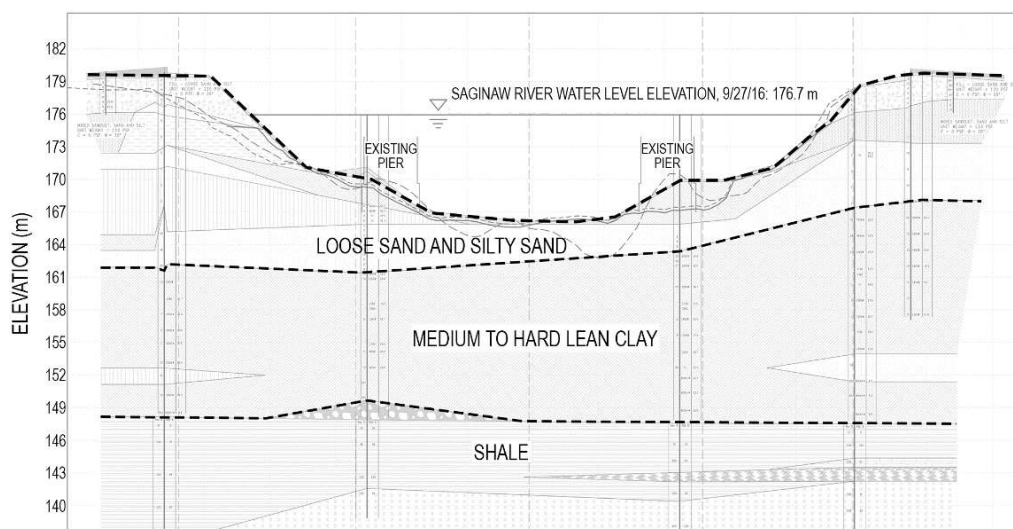

Figure 2. Subsurface soil profile at the bridge site, © 2020 MDOT. Modifications by FHWA.

The clay layer started very stiff at the right overbank, with standard penetration tests (SPTs) producing *N*-values of 30 at an elevation of 167.6 m (550 ft). However, these values dropped quickly to around 10 at an elevation of 164.6 m (540 ft). Below that elevation, the clay had similar *N*-values across the entire channel, varying between 7 and 12 before increasing again near the shale layer.

MDOT calculated the scour depths using the current standard practice, which assumes a uniform layer of riverbed material in this case, 0.1 mm (0.039 in) sand (Arneson et al., 2012). The total pier scour depth, which considered both contraction and pier scour, was 11 m (36 ft) for Q_{100} and 12.5 m (41 ft) for Q_{500}, which seemed excessive. The channel thalweg elevation is around 167.6 m (550 ft). Therefore, these scour depths correspond to 156.7- and 155.1-m (514- and 509-ft) elevations, respectively. The proposed steel piling will need to be driven to an adequate bearing layer, that is, the shale bedrock. The estimated pile lengths are about 24.4 m (80 ft) below the bottom of the pier footing and 29 m (95 ft) below the abutment footings. The combination of deep scour and large vertical and horizontal loads requires massive driven piles. The preliminary design evaluated 200 large (HP 18×204) driven piles per pier. It is common in Michigan to drive HP 14×73 piles for large structures. HP 18×204 would be a specialty pile that requires the consultant to modify the existing equipment or get a larger one to install the piles for this project.

MDOT would like to know whether the thick layer of lean clay could potentially provide sufficient erosive resistance to the design floods and reduce the original values of the design scour depths. Cohesive materials, such as clay, are typically more resistant to scour than sandy materials due to their higher critical shear stresses. Still, obtaining the critical shear value of cohesive materials through erosion testing is preferable (Arneson et al., 2012). Therefore, the Federal Highway Administration (FHWA) established a Transportation Pooled Fund (TPF) study, TPF-5(461) *Soil and Erosion Testing Services for Bridge Scour Evaluations* (FHWA, 2020). This study is a collaborative effort between the Hydraulics and Geotechnical Laboratories at Turner-Fairbank Highway Research Center (TFHRC) and includes support from the FHWA Resource Center. The study allows state departments of transportation to partner with FHWA to perform the soil and erosion testing required to determine material properties, such as critical shear stress, which are needed to calculate scour depths more accurately. The Lafayette Avenue Bridge was an excellent candidate for this TPF study. If the erosion test could help define the erodibility of the clay at this site and reduce the calculated scour depths, then the size and/or the number of required piles would likely be reduced.

In addition to providing soil erosion testing, the FHWA Hydraulics Laboratory used physical and numerical modeling to simulate the three-dimensional flow around the Lafayette Avenue Bridge's wide bascule piers. The physical modeling of the bridge piers and abutments in a flume calibrated and verified the computational fluid dynamics (CFD) models. The flume scour tests also provided incremental scour bathymetries. These bathymetries were imported into CFD to compute the nominal water loads at incremental scour depths, thus developing the hydraulic load decay functions.

NextScour Research Initiative

FHWA is developing NextScour, a next-generation scour research initiative to improve scour analysis and provide more accurate scour depth estimates for bridge foundation design. NextScour considers the two major scour components: hydraulic loads and the erosional resistance of soils (Shan et al. 2021a). Traditional hydraulic analysis typically uses one- and two-dimensional (1D and 2D) models to calculate flow parameters at a proposed bridge site that are then used for scour calculations. NextScour proposes using three-dimensional (3D) CFD modeling to compute bed shear stresses directly at the bridge site. 1D and 2D modeling use composite channel friction, including vegetation, bed irregularity, and surface friction due to channel sediments, to calculate an average bed shear stress, whereas 3D CFD directly models the effect of surface friction due to channel sediments. The average bed shear stresses from 1D and 2D modeling are usually larger than those from 3D CFD. Therefore, CFD models will generate factors of bed shear stresses for 1D and 2D models to determine the shear stresses governing soil erosion. Hydraulic load decay functions are developed with laboratory flume scour tests and accompanying CFD modeling within the scour hole.

Regarding the aspect of resistance, NextScour focuses on improving estimates of the critical shear stress of layered soils, especially cohesive soils, through erosion testing. FHWA has developed the Ex-situ Scour Testing Device (ESTD), the In-situ Scour Testing Device (ISTD), and the Portable Scour Testing Device (PSTD) to estimate the erodibility of cohesive soil samples and their corresponding critical shear stresses (Shan et al. 2011, 2015, 2018, and 2021a; Zinner et al., 2016). Additional geotechnical tests are also conducted on these samples to fully characterize the soils tested.

Scour design variables inherently include several uncertainties, such as peak flood occurrence, channel roughness, riverbed materials, and scour equation uncertainties. Thus, NextScour also investigates a probabilistic approach that considers the uncertainties of water loads and the soil resistance, and determines scour exceedance probabilities.

HYDRAULIC MODELING

Hydraulic modeling for this case study aimed to predict the flow depths, velocities, and bed shear stresses at the bridge. MDOT provided the 1D Hydrologic Engineering Center's River Analysis System (HEC-RAS) model and the Sedimentation and River Hydraulics Two-Dimensional (SRH-2D) model of the project. The light detection and ranging (LiDAR) topography was exported from the 2D model to construct the 3D CFD computational domain. The 3D model included an area of approximately 305 m (1,000 ft) upstream and downstream of the bridge in the east channel (Figure 3). It also contained the computer-aided design model of the proposed bridge.
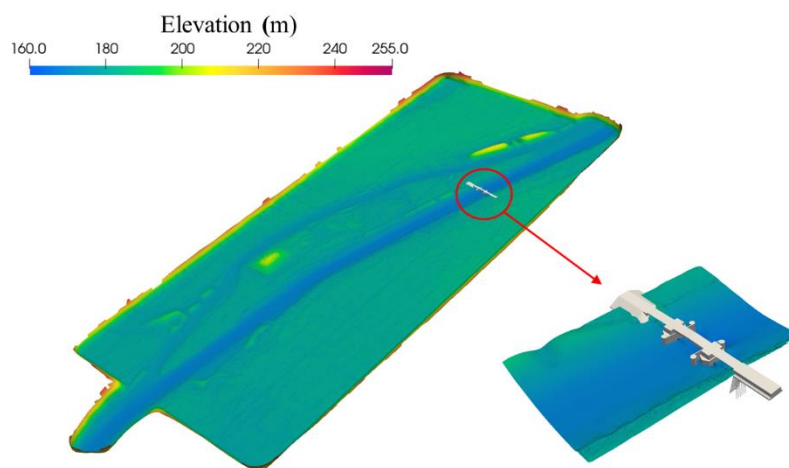

Figure 3. LiDAR topography and the CFD simulation domain with the proposed bridge model, Source: FHWA.

The volume of fluid (VOF) method was first adopted to simulate two-phase flow (air and water) in the 3D domain and to better predict the water surface. The domain had a uniform velocity inlet and pressure outlet. The riverbed was modeled as a rough wall with a roughness height of 0.2 mm (0.008 in), which was two times the D_{50} of the riverbed surface sand. Corresponding single-phase hydraulic models were developed to simplify the simulations. A single-phase model does not incorporate air in the simulation. Instead, a top wall is placed at the expected water surface elevation (WSE) (obtained from the HEC-RAS model). It is set as a symmetrical boundary to simulate the water surface. In the single-phase model, the inlet was defined as a discharge inlet, whereas the outlet boundary and riverbed were identical to the VOF model. An unsteady Reynolds-averaged Navier-Stokes (URANS) solver with a *k*-epsilon turbulence model was selected to solve the momentum equations.

Initial test runs showed that the VOF and single-phase models produced similar results, so the single-phase model was adopted for the remaining CFD simulations. The simulation results of flow velocities and bed shear stresses of the single-phase model were compared with SRH-2D results. As shown in Figure 4, velocity distributions between both models were similar. The upstream approach velocity in each case was almost identical. But the water flow around the piers was different in the SRH-2D model because it cannot accurately simulate the 3D flow pattern around the bridge. Figure 5 compares the bed shear stresses. The SRH-2D model showed relatively larger bed shear stresses upstream and downstream of the bridge compared to the CFD model but had comparable stresses closer to the bridge.
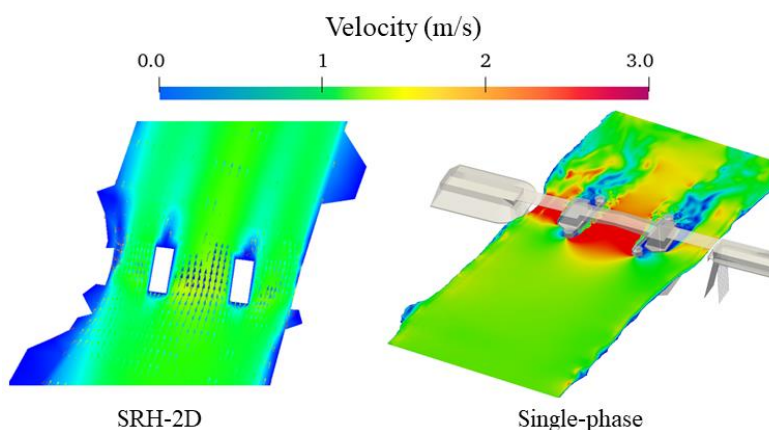

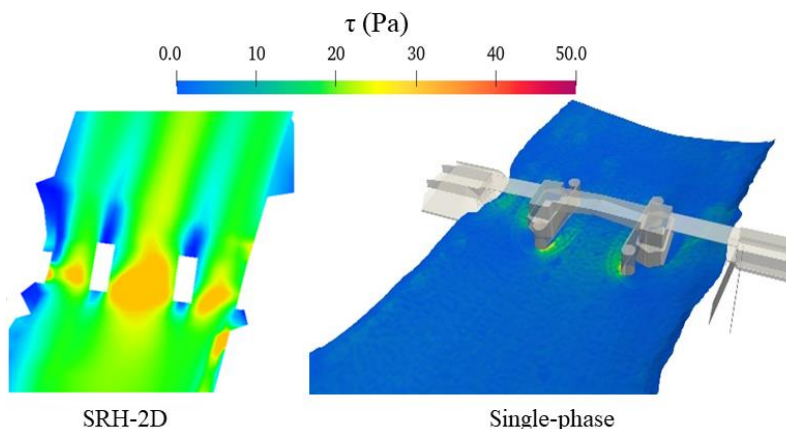*Figure 4. Velocity distributions of SRH-2D and single-phase CFD models, Source: FHWA.*

Figure 5. Bed shear stress distributions of SRH-2D and single-phase CFD models, Source: FHWA.

Nominal CFD Bed Shear Stress

The riverbed in a CFD model is composed of millions of cells, with each cell outputting a single shear stress value. To determine a relevant average shear stress value adjacent to the bridge pier, an area of interest must be identified. Then the

shear stress values from cells in that area can be averaged. A flow separation zone forms when water passes an obstruction. Bed shear stresses in the separation zone are amplified compared with upstream approach shear stresses, which initiate the scour process. CFD simulation results indicated that the flow separation zone is similar in size to the blockage area due to the obstruction. The blockage area is equal to the obstruction width multiplied by the flow depth. Therefore, the flow separation zone is the area of interest where bed shear stresses are averaged to determine the nominal shear stress due to the obstruction. This averaged nominal bed shear stress can then be compared with shear stress calculated from HEC-RAS output flow parameters to compute the shear stress modification factor.

For the Lafayette Avenue Bridge, the proposed upstream cylindrical fenders had the deepest scour hole from the flume scour observations. The blockage area was the fender diameter multiplied by the flow depth in this case. Guo et al. (2012) reported that scour begins at 45 to 75 degrees relative to the flow direction around a cylindrical pier. Therefore, the screening area where all shear stresses were considered in determining the nominal shear stress was determined to be upstream of the fender centerline and below the pile cap of the pier at an elevation of 170 m (557.7 ft) (Figure 6(a)). The shear stresses in the screening area were ranked from largest to smallest until the accumulative cell area equaled the blockage area. Area-weighted average shear stress was calculated to be the nominal bed shear stress (Figure 6(b)). Table 1 lists the nominal shear stresses at the two fenders for various flows.
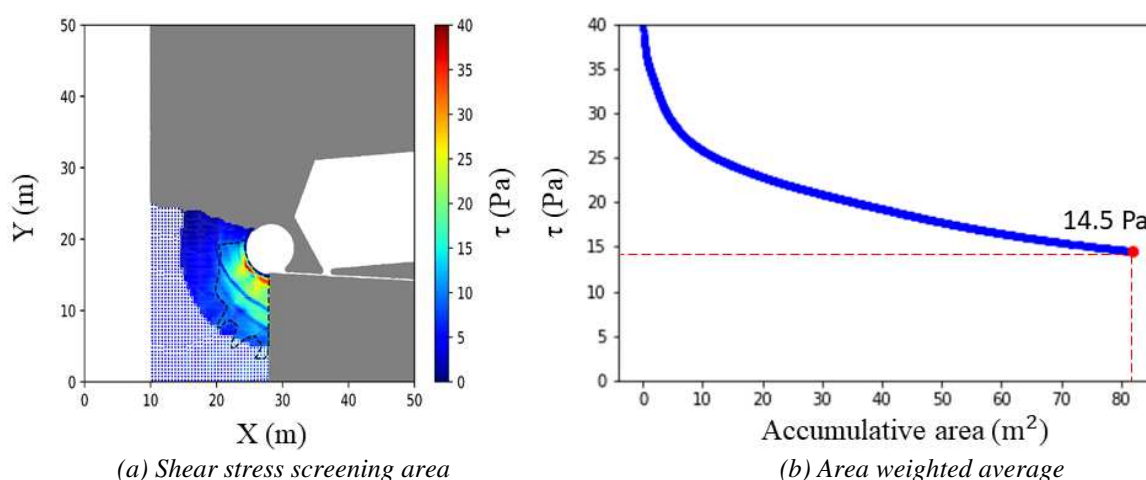

(a) Shear stress screening area   *(b) Area weighted average*

Figure 6. Calculation of the nominal CFD bed shear stress, Source: FHWA.

Table 1. Flow conditions and representative shear stresses for different flows.

Flow	Flow Rate (m^3/s)	Water Surface Elevation (m)	Average Velocity (m/s)	Blockage Area (m^2)	Shear Stress at Left Fender (Pa)	Shear Stress at Right Fender (Pa)
Q_{10}	1,211.5	177.1	1.3	80.4	8.2	7.1
Q_{50}	1,543.6	177.2	1.7	81.4	12.1	11.6
Q_{100}	1,680.9	177.2	1.8	81.8	14.5	14.1
Q_{500}	1,985.9	177.4	2.1	83.0	20.2	19.7
$Q_{2,000}$	2,245.4	177.5	2.3	83.5	26.2	24.5

CLAY EROSION TESTING

MDOT collected 27 Shelby tube soil samples in three boreholes at the bridge site. The first two boreholes (BB101 and BB102) were downstream of the bridge at each of the existing piers, and the third borehole (MB1) was located at the left abutment upstream of the bridge. MDOT shipped the Shelby tubes to the Hydraulics Research Laboratory at TFHRC for erosion tests using the ESTD. The erosion testing results determined a critical shear stress distribution of the clay layer below 161.5-m (530-ft) elevation and was later used for the probabilistic scour analysis.

ESTD

The ESTD (Figure 7) measures the erodibility of cohesive soil in a Shelby tube under well-controlled flow conditions. It integrates a robotic arm, an underwater laser scanner, two filter cylinders, a hydraulic piston, and a direct shear sensor (Shan et al., 2011, 2021b). The erosion test process is fully automated. The enclosed rectangular acrylic test channel measures 0.9 m (3 ft) long, 120 mm (4.7 in) wide, and 19 mm (0.75 in) high. The maximum flow rate is 14 L/s (0.5 ft^3/s), which translates to a maximum average flow velocity of 6.1 m/s (20 ft/s) in the testing channel. During an erosion test, the underwater laser scanner mounted on a robotic arm (Figure 8) scans and sends the quasi-instantaneous soil surface change due to erosion to the control program. The control program includes an automated feedback loop to provide feedback to advance the hydraulic piston, which extrudes soils out of Shelby tubes to ensure the soil surface remains flush with the channel bottom. The innovative electromagnetic shear stress sensor (Shan et al., 2015) can instantaneously measure flow shear stresses on soil samples during the erosion process and is located upstream of the Shelby tube soil sample. The two filter cylinders clean water in the system for observation and video recording. The control program records the flow rate, shear stress, soil surface elevation, and piston positions. Shan et al. (2021b) outlined the detailed ESTD test procedures.
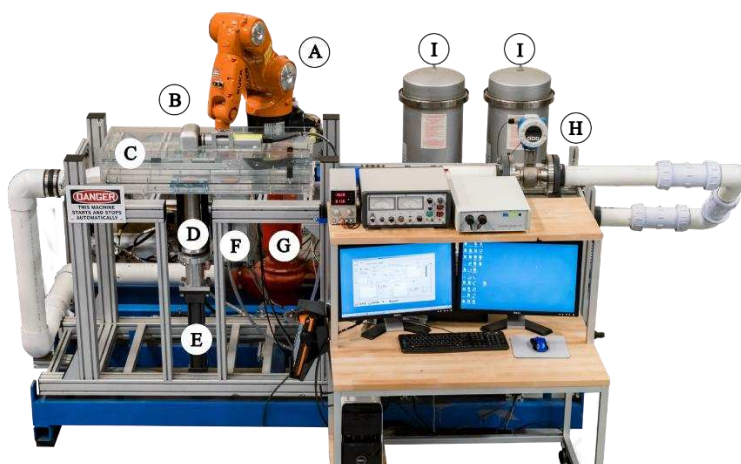
A = Robotic arm; B = laser scanner; C = flow channel; D = 3-in Shelby tube soil; E = hydraulic piston; F = shear sensor; G = flow pump; H = flow meter; and I = filter cylinder.

Figure 7. ESTD, Source: FHWA.

Figure 8. Laser scanner scanned soil surface and digitized soil surface (inset), Source: FHWA.

For ESTD erosion tests, one or two 305-mm (1-ft) sections were cut from each Shelby tube, usually from the tube bottom. On top of each tube sample, laboratory engineers performed the strength tests by using a pocket penetrometer (PP) and a shear vane tester. After extracting and removing the disturbed soil surface from these strength tests, laboratory engineers conducted erosion tests on the remaining soil in the tube. Only the top 228 to 255 mm (9–10 in) of soil were tested because the bottom 51 to 75 mm (2–3 in) had a greater propensity to dislodge from the tube in the flow due to decreased friction

surface area between the soil and the Shelby tube. Table 2 shows the elevation ranges of ESTD test tubes, strength test results, and water content of each Shelby tube sample. FHWA's Geotechnical Laboratory provided soil classifications for three of the tested samples including MB1 ST1 and ST2, and BB102 ST14, and determined they were all low plasticity clay. They tested an additional six samples not included in ESTD testing and found they all were also low plasticity clay.

Table 2. Elevations of ESTD erosion test samples and basic soil geotechnical information.

Tube No.	Elevation (m)	Elevation of Test Tube (m)	Elevation of Strength Test (m)	PP (kPa)	Vane Shear Strength (kPa)	Water Content (%)
MB1 ST1	160.4–159.6	159.9–159.6	159.9	119.7	64	8.7
MB1 ST2	159.6–158.8	159.1–158.8	159.5	105.3	40	13.6–14.9
MB1 ST4	158.1–157.3	157.6–157.3	157.9	143.6	48	20.5–23.4
MB1 ST8	155–154.3	154.6–154.3	154.6	71.8	36	28.2–29.8
BB101 ST12	159.1–158.5	158.7–158.4	158.7	80	22	14.9
BB101 ST15	154.7–154	154.3–154	154.6	76.5	44	23.5
BB102 ST5	165.5–164.7	165.2–164.9	164.9	57.5	40	28.2
BB102 ST11	160.9–160.1	160.5–160.2	160.5	167.6	86	14.9–17.7
BB102 ST14	157.9–157.1	157.4–157.1	157.5	167.6	62	26.6

ST= Shelby tube sample.

The typical duration of an erosion test for one flow rate per velocity setting is 10 minutes. A linear best fit line is applied to the erosion data (recorded position of the soil surface along with time) for each flow rate, and the slope represents the erosion rate. Flow shear stresses on soil samples are recorded separately from the erosion tests by using 15-mm (0.6-in) -thick soil samples confined in stainless steel rings. The ring is mounted to a small bowl that attaches directly to the sensor disk. The bowl's interior features a raised circular platform, which pushes the soil out about 2 mm (0.08 in) above the edge of the ring. Once mounted on the shear sensor, the sensor disk height is adjusted until the soil surface is flush with the test channel surface. With recorded shear stresses and erosion rates, the critical shear stress of the soil can be extrapolated.

Figure 9 shows that all nine Shelby tube samples had higher erosion rates as the flow rates increased (increased shear stresses), which follows the physical relationship between the erosion rate and the flow shear stress (Eq. 1). However, Figure 9 also reveals that Shelby tubes ST5 from borehole BB102 had much higher erosion rates at the same shear stresses than other tubes, indicating lower critical shear stresses for this tube sample. The subsurface soil profile (Figure 2) indicates ST 5 was not in the clay layer, and therefore the soil erosion data were excluded in the critical shear stress analysis. Data in Figure 9 is very scattered and cannot be certainly fitted using a single curve, making it more reasonable to get the distribution instead of a deterministic value of the critical shear stress.
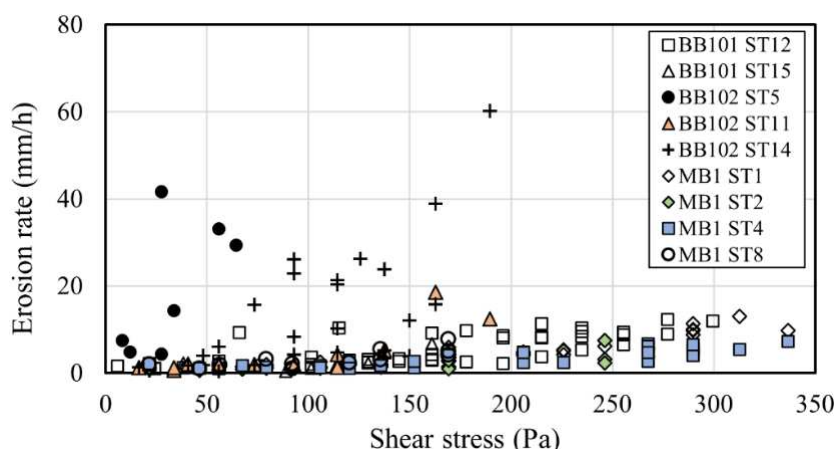

Figure 9. Erosion rates of nine Shelby tube samples with a 10-minute time window, Source: FHWA.

Critical Shear Stress Distribution

A power function was applied to describe the erosion function of the cohesive soil tested:

$$\dot{e} = k_a \tau^{k_b} \tag{1}$$

Where $\dot{e}$ is erosion rate in mm/h, τ is shear stress in Pa, and k_a and k_b are constants.

By taking the logarithm with base 10 of both sides, Eq. 1 converted to a linear relationship, and a linear best fit was applied to the data to obtain constants k_a and k_b. After fitting both constants, the critical shear stress was defined as the shear stress when the erosion rate equaled 0.1 mm/h (0.0039 in/h) which matched the definition used by Briaud et al. (2011).

$$\log(\dot{e}) = \log(k_a) + k_b \times \log(\tau) \tag{2}$$

To increase the number of data points, the erosion curve was divided into smaller time windows. The size of the windows was 4 minutes, with a 2-minute overlap between adjacent windows. A linear best fit function was applied to the erosion curve data in each window, where the slope of the linear fit was equal to the erosion rate. For very low flows, where erosion may not be detectable by the laser, a lower boundary for erosion was set at 0.016 mm/h (0.00063 in/h), which was based on the resolution of the laser scanner. In total, 1,127 erosion data points were collected (Figure 10). The solid line represented the linear fit function. With the corresponding fitted constants k_a of 0.00033 mm/h (0.000013 in/h) and k_b of 1.89, the critical shear stress was calculated to be 20.5 Pa (0.43 psf).
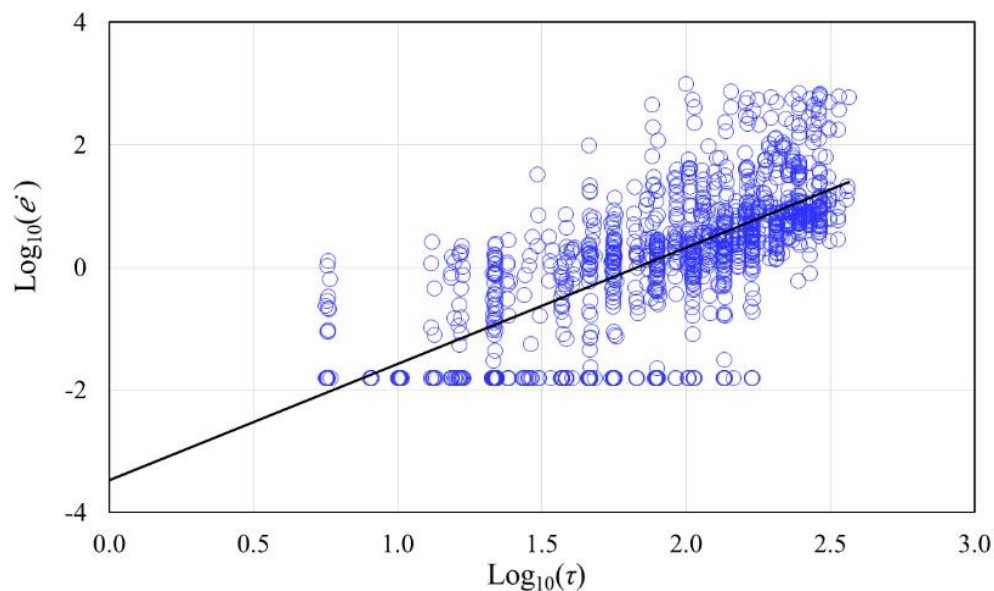

Figure 10. Logarithm of erosion rate versus logarithm of shear stress, Source: FHWA.

A probabilistic scour approach was also considered to calculate the distribution of the critical shear stress. Several methods were considered, but ultimately a bootstrapping methodology was adopted (Stine, 1989). A script randomly selected 40 out of the 1,127 total data points, and then a linear best-fit function was applied to these 40 data points to calculate a corresponding critical shear stress. This process was then repeated 50,000 times to get a distribution of 50,000 critical shear stresses (Figure 11). The two dashed lines represent the 95 percent confidence limits of the mean critical shear stress, and the solid line is the mean linear function of the 50,000 fittings. Figure 12 plots the histogram of all 50,000 critical shear stresses. The mean value of the critical shear stresses was 20.5 Pa (0.43 psf), which matched the value calculated previously for the entire 1,127-point dataset. The standard deviation was 6.56 Pa (0.14 psf), and the coefficient of variation (COV) was 0.32. Both mean and COV were used as the critical shear stress distribution parameters. Because the erosion rates follow a lognormal distribution, the distribution of the critical shear stress was also assumed lognormal.
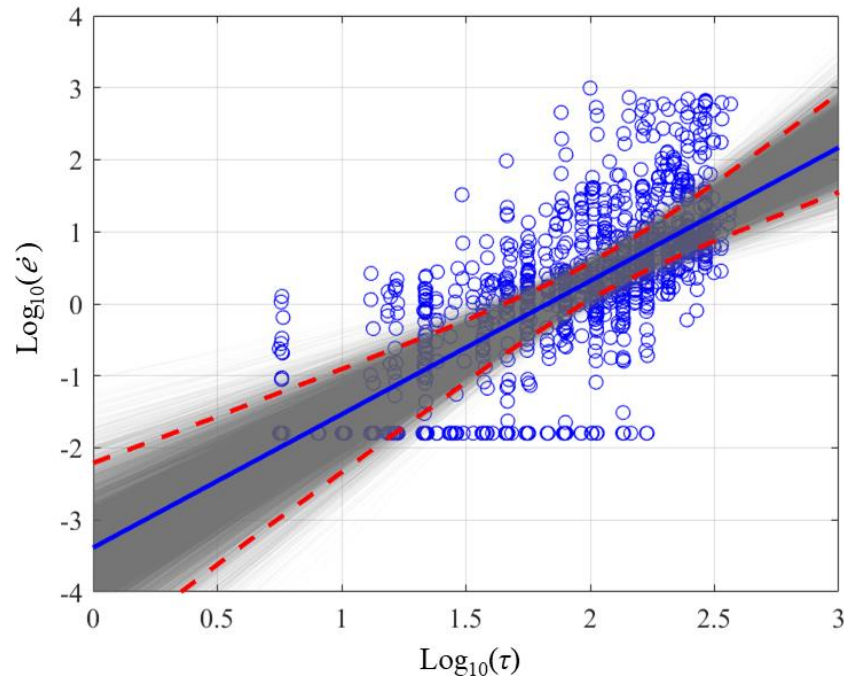
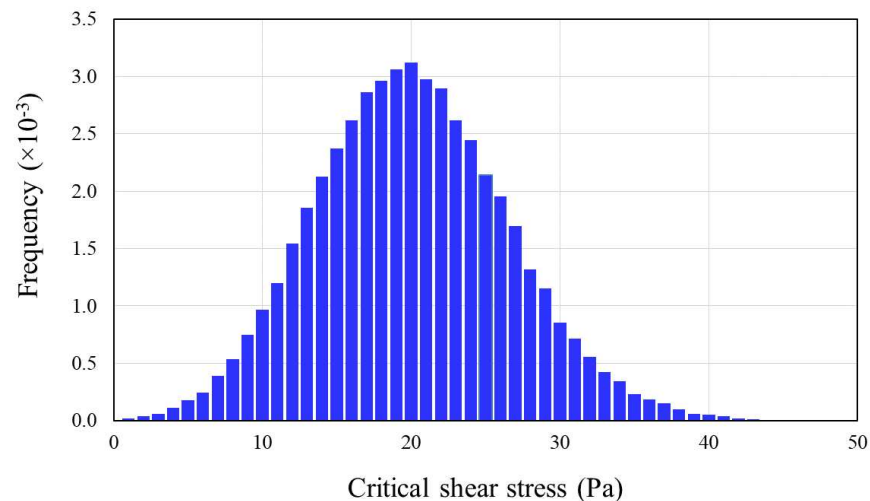*Figure 11. Bootstrapping technique showing 50,000 linear fittings, Source: FHWA.*

Figure 12. Histogram of the 50,000 critical shear stresses, Source: FHWA.

DECAY FUNCTIONS

It is logical that the water load is amplified at the flow obstruction. When the amplified shear stress exceeds the critical shear stress of the bed materials, scour starts. As the scour hole deepens, the load from the flow decays. It further reduces to a value that equals the critical shear stress of the bed materials when scour reaches the equilibrium condition. This process can be described by the decay function, which calculates the shear stress at the flow obstruction with a given scour depth (Eqs. 4 and 5). For this case study, the decay function was developed with laboratory flume scour tests and accompanying CFD modeling within the scour hole. Physical experiments were conducted in the Hydraulic Research Laboratory's 1.83-m (6-ft)-wide Multifunctional Flume System (MFS) using scaled Lafayette Avenue Bridge models. Multiple model configurations were tested, including pier with embankment and abutment. Flume tests ran for a minimum of 70 h but could last up to 120 h and were paused at regular intervals to scan the bathymetry that is to measure the incremental progress of the scour hole. These scans were then used to calculate the decay of the hydraulic loads and calibrate the CFD models of the experiments.

Flume Scour Tests

The Froude criterion was used to determine the geometric scale of the model because the governing force is gravity, and open channel flow aspects dominate. A geometric scale factor (model:prototype) of 1:50 was selected for the flume tests, which provided a reasonable experimental flow depth and an appropriate model size of the bridge components without significant influence from the flume sidewalls. At this scale, the entire bridge was separated into the following two models:

- Set L: left half-bridge with pier and abutment.

- Set R: right half-bridge with pier and abutment.

The model pier was about 335 mm (1.1 ft) wide, and the model fender cylinder had a diameter of 152.4 mm (6 in). The prototype river cross sections were simplified and reproduced in the MFS. Four cross sections upstream of the bridge, two cross sections at the bridge, and five cross sections downstream of the bridge were exported from the LiDAR topography. The average main channel riverbed elevation from these cross sections was 167.7 m (550.2 ft). The average left and right bank slopes were 0.13 and 0.22, respectively, with a standard deviation of 0.03.

Figure 13 shows the simplified and scaled model setups in the MFS looking downstream. The 7.5-degree skew angle was kept in the scaled models. The floodplain at the left abutment had an elevation of 175.6 m (576.3 ft). The horizontal distance between the main channel edge and the left floodplain edge measured approximately 47.1 m (154.6 ft). This resulted in a left bank slope of 0.169 (9.6-degree). Similarly, the right floodplain had an elevation of 177.4 m (582 ft), which resulted in a right bank slope of 0.25 (14-degree). For both sets L and R, a minimum distance of 600 mm (2 ft) was maintained between the fender and the MFS wall to minimize any contraction effects between both.
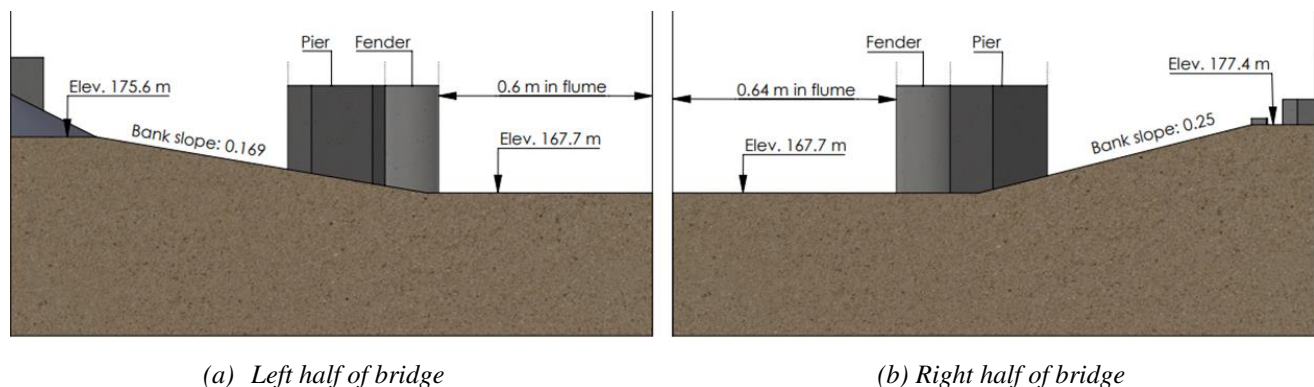

(a) Left half of bridge   *(b) Right half of bridge*

Figure 13. Scaled bridge models in MFS, Source: FHWA.

Since both test setups were part of a compound channel, two transition structures were designed and 3D printed to ensure the rectangular channel smoothly transitioned to the compound channels without introducing scour at the very upstream of the sand recess section, which was about 0.4 m (1.6 ft) deep. Both sets modeled half of the bridge, but the two models were not split from the centerline of the main channel. Therefore, the flow rate percentage of Q_{100} was estimated from the CFD simulation of the full-scaled geometry by using both single-phase and VOF models. The flow rate ratio of Sets L and R was 64.1 percent and 59.4 percent, respectively, indicating that the two model sections partially overlapped at the center of the channel.

The Saginaw riverbed has very fine sands with a D_{50} of 0.1 mm (0.004 in), which are impossible to scale down in flume tests. So, uniform sands with a D_{50} of 1.15 mm (0.045 in) were used instead. The flume-scale flow rate, flow depth, and upstream approach velocity (V_{Q100}) were calculated from the scaling factor, Q_{100} discharge (1,607 m³/s; i.e., 56,770 cfs), and WSE (178.5 m; i.e., 585.5 ft). Table 3 lists the flow conditions. As shown in the table, two different approach velocities ($V_{approach}$) were used for each set to ensure the scour depth was accurately measured and the effect of the flume walls was minimized. The critical velocity for the 1.15-mm (0.045-in) sand under the 21.6-cm (0.71-ft) flow depth was calculated to be 0.5 m/s (1.6 ft/s), and the approach velocity was about 30 to 38 percent of the critical velocity, thus ensuring a clear-water scour condition.

Table 3. Flow conditions of flume scour tests.

Cases	Flow Rate (L/s)	Water Depth (cm)	Scaled V_{Q100} Approach (cm/s)	$V_{approach}$ (cm/s)	V Ratio (%)	Run Time (hr)	Scour Depth (cm)
Set L.1	59.5	21.6	14.9	14.9	100	70	5.5
Set L.2	70.8	21.6	14.9	17.7	120	124	11.6
Set R.1	59.5	21.6	13.7	14.9	108	87	6.1
Set R.2	65.1	21.6	13.7	16.5	120	85	10.7

The experiment was prepared by positioning the models in MFS according to the design drawings. The sediment was then placed around the models, compacted, and shaped with the assistance of a robotic arm mounted on a linear carriage over the MFS. The robotic arm could be programmed to repeatedly form complex sediment formations, including the channel slope. Each experiment started by scanning the initial bathymetry using an underwater laser scanner. Water was slowly introduced into the flume with a near-zero flow rate to minimize disturbance of the bed material. The flow depth was then increased until the scanner was submerged. Once the laser scan was completed, the experiment began by decreasing the flow depth while gradually increasing the flow rate. Each test required two runs. The first run was to establish the equilibrium scour depth, the total run time was logged in Table 3, and the final bathymetry was scanned. Then a second run was repeated and paused at approximately 20, 40, 60, and 80 percent of the equilibrium scour depth. When the targeted scour depth was reached, the flow was reduced to standing water, and then the laser scanner collected the bathymetry. After the scan was finished, the flow resumed, and the run continued until the next incremental scour depth was reached. Figure 14 shows a typical scanned bathymetry in the form of a 3D point cloud.
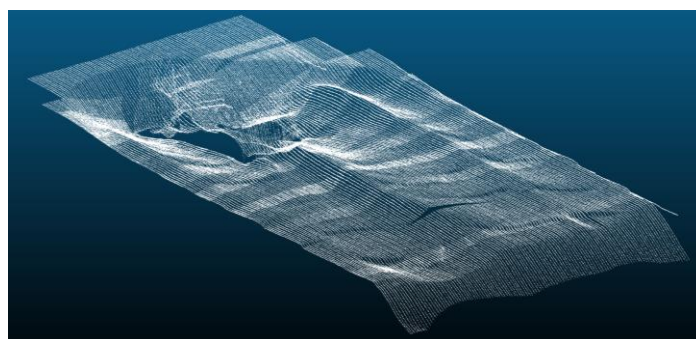

Figure 14. A typical scour bathymetry scanning result, Source: FHWA.

Figure 15 shows a typical scour depth development over time, indicating that the scour reaches equilibrium after about 80 h. Figure 16 shows the equilibrium scour hole around the pier and fender. Water flows from right to left, and the deepest scour hole appears upstream of the upstream fender cylinder.
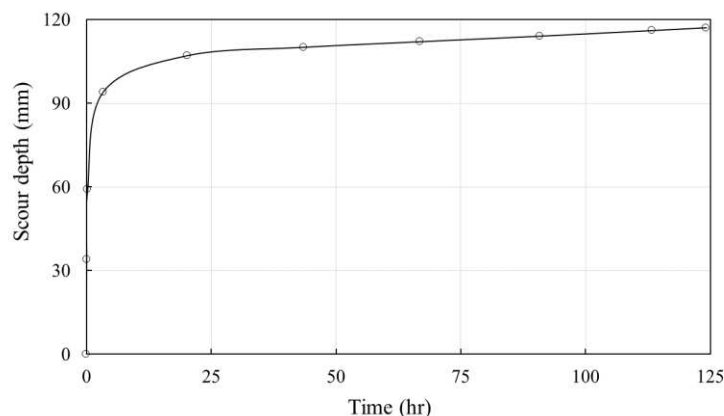

Figure 15. Scour depth progress of Set L.2, Source: FHWA.

(a) Set L   *(b) Set R*

Figure 16. Final scour hole around the pier and fender, Source: FHWA.

Decay Function Development

The incremental scour bathymetries collected by the laser scanner were post-processed and exported into CFD to compute the nominal bed shear stress to develop the decay function. The nominal bed shear stress at each incremental scour bathymetry was calculated by following the procedure outlined in the Nominal CFD Bed Shear Stress section. Figure 17 illustrates the bed shear stress distributions for Set L.2 on the scanned incremental scour bathymetries. The figure shows that two red zones of high shear stress appear on either side of the fender and pier at the initial riverbed. As the scour hole deepens, shear stress magnitude decreases until most of the area around the fender and the pier is in light green, close to the critical shear stress of the 1.15 mm (0.045 in) sands. This reflects a clear trend of shear stress decay as the scour hole deepens.

The nominal bed shear stresses at incremental scour depths were normalized by the upstream approach shear stress, τ_a. Since the flume tests had zero slope, the approach shear stress was computed by using Eq. 3 with the friction factor f obtained from Moody's diagram. The Reynolds number and relative roughness were needed to determine the friction factor. For rectangular channels, the character length in the Reynolds number is the hydraulic diameter, that is, four times the hydraulic radius. The relative roughness is the ratio of $0.5D_{50}$ to the hydraulic diameter.

$$\tau_a = \frac{1}{8}f\rho V^2 \tag{3}$$

Where ρ is the water density and V is the average approach velocity. The incremental scour depths were normalized by the obstruction width, *B,* which was used in the Nominal CFD Shear Stress section to calculate the blockage area. Since scour mainly occurs around the upstream fender cylinder for Sets L and R, the projected width was set as the fender diameter. An exponential function, $\frac{\tau}{\tau_a} = a\,exp(-b\,\frac{y_s}{B})$, was fitted through the data for all four cases (Figure 18), where τ is the decayed nominal shear stress at a certain scour depth, a and b are fitting constants, and y_s is the incremental scour depth.

Figure 18 indicates that the data from these four cases generally align, and the best-fit and design decay functions are given in Eqs. 4 and 5. Shan et al. (2016) used a reliability index (RI) to measure the reliability and accuracy of an equation. The same RI analysis was performed here to make sure the design decay function had a RI of 2.0. That resulted in the design equation being the best-fit one multiplied by a safety factor of 1.23.

$$\frac{\tau}{\tau_a} = 7.14exp(-0.81\,\frac{y_s}{B}) \tag{4}$$

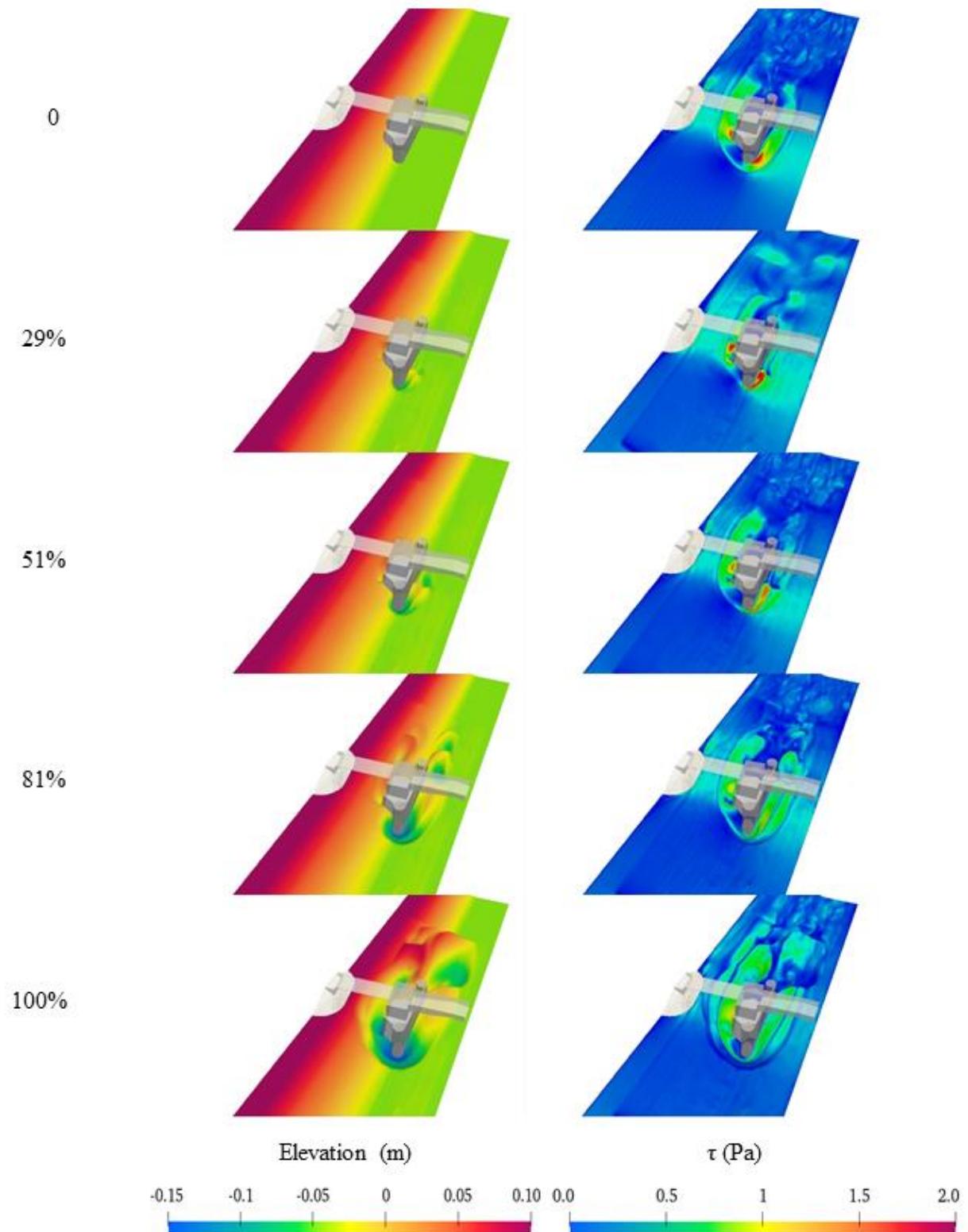$$\frac{\tau}{\tau_a} = 8.78exp(-0.81\,\frac{y_s}{B}) \tag{5}$$

Figure 17. Bed shear stress distributions at incremental scour depths, Source: FHWA.
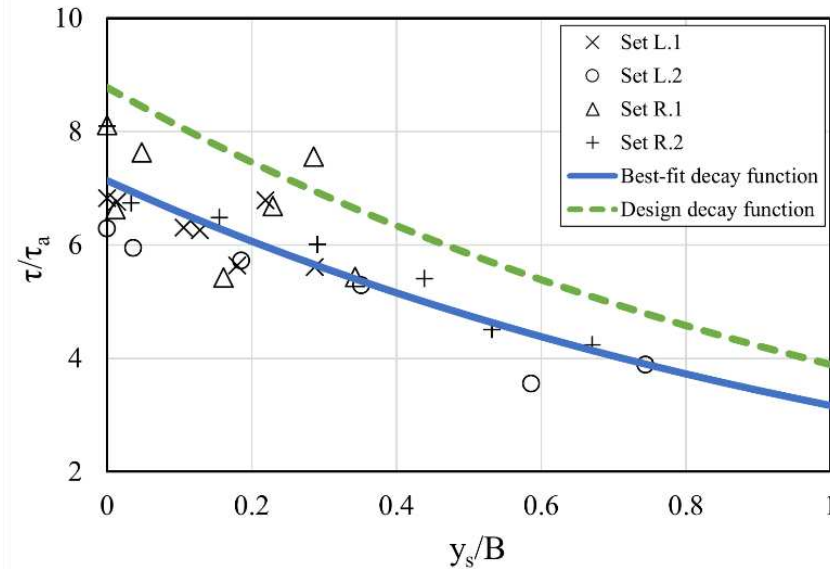
Figure 18. Decay function for MDOT Sets L and R, Source: FHWA.

Both decay functions are site-specific for the unique pier and fender configuration of this MDOT project. Additionally, the decay functions were developed under clear-water conditions. Therefore, they may not be applicable for live-bed scour conditions. Clay erodes in the form of chunks containing multiple fine clay particles, and it is reasonable to assume that scour in clay is similar to the clear-water scour condition.

Although Eqs. 4 and 5 were derived from flume scour tests of 1.15-mm (0.045-in) sand, it is assumed that decay functions are independent of the grain size. While it is true that the configuration of the scour hole depends on grain size, the decay function only considers the proportional depth compared to the total equilibrium scour depth for a specific flow condition. Annandale (2006) summarized data collected at TFHRC Hydraulics Research Laboratory from flume scour experiments using different sands and piers. Sand grain sizes included 1.2 mm (0.05 in), 2.4 mm (0.09 in), and 5 mm (0.2 in), and pier shapes included cylindrical, square, and round-nose. When a decay function was derived based on this data set, it was found that the curve was insensitive to the various sand sizes. Nevertheless, a future study could be conducted to collect more data about the effect of grain sizes and soil types on the scour hole configuration, the resulting shear stresses, and the decay function.

DETERMINISTIC SCOUR ANALYSIS

The current scour calculation practice uses deterministic equations. Therefore, the deterministic scour analysis was conducted following the same logic. CFD nominal shear stresses (Table 1) represent the nominal hydraulic loads on the riverbed. For the design loads, an equation target reliability of 2.0 was selected, resulting in an amplification of the nominal loads by a factor of 1.23. The factor equals the ratio between the design and best-fit decay functions. For design, the nominal shear stresses for Q_{100} increased from 14.5 Pa (0.3 psf) (Table 1) to 17.8 Pa (0.37 psf), and for Q_{500} from 20.2 Pa (0.42 psf) to 24.8 (0.52 psf) Pa. To account for uncertainties in the soil erosion resistance, the mean critical shear stress (τ_{mean}, nominal critical shear stress) was reduced by one standard deviation, decreasing the nominal critical shear stress from 20.5 Pa (0.43 psf) to a design critical shear stress (τ_{design}) of 13.9 Pa (0.29 psf). The design decay function (Eq. 5) yields decaying shear stresses at incremental scour depths. Scour stops at a scour elevation where the shear stress (hydraulic load) from the decay function is smaller than the design critical shear stress of the clay.

Figure 19 reveals how the shear stress decays with elevation for both the Q_{100} and Q_{500} flood events. The top elevation of 167.6 m (550 ft) on the plot is equal to the elevation of the thalweg of the river. The nominal shear stress of the Q_{100} event was 17.8 Pa (0.37 psf) at elevation 167.6 m (550 ft) and decayed to 9.3 Pa (0.19 psf) at elevation 161.5 m (530 ft), which is where the clay layer starts. Similarly, the Q_{500} event decayed from 24.8 Pa (0.52 psf) to 13 Pa (0.27 psf) for the same elevations. At elevation 161.5 m (530 ft), both shear stresses were less than the design critical shear stress of the clay, which was 13.9 Pa (0.29 psf). Therefore, it was determined that the clay layer would stop the scour for both flood events.
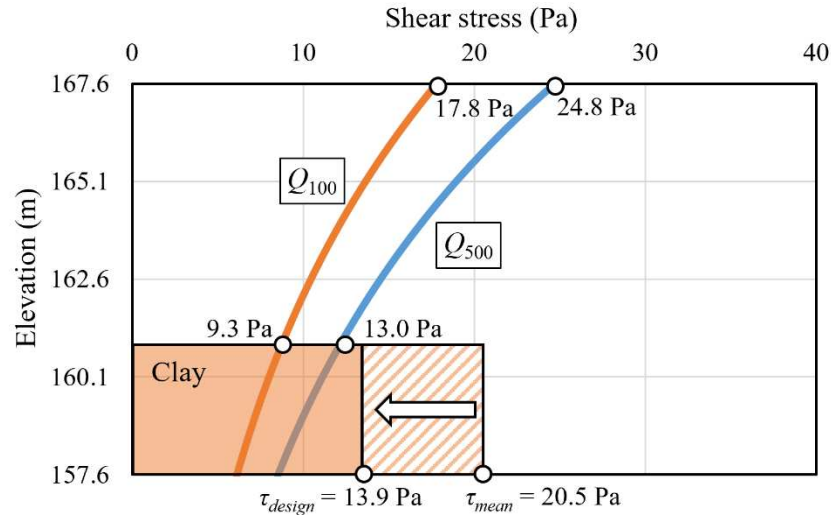
Figure 19. Deterministic scour analysis using decay function and clay resistance for Q_{100} and Q_{500}, Source: FHWA.

PROBABILISTIC SCOUR ANALYSIS

Concept of Load and Resistance in Scour Design

In scour, the load refers to the bed shear stress produced by the flow, and the resistance is the critical shear stress of the soil. When the flow-induced bed shear stress is larger than the critical shear stress of the soil, scour occurs. Probability of exceedance, $P_{e,scour}$, represents the probability of the scour going beyond a scour depth. Figure 20(a) shows the concept of load (L) and resistance (R) distribution and $P_{e,scour}$ for a preset scour depth. The load distribution is calculated from a Monte Carlo simulation by considering various uncertainties in the flood event. The distribution of the resistance, τ_c, is obtained from soil erosion tests. The R minus L curve represents the difference between the load and resistance distributions. When this function is negative—represented by the shaded area—the result is $P_{e,scour}$. A relationship between $P_{e,scour}$ and incremental scour depths can be established, as shown in Figure 20(b).
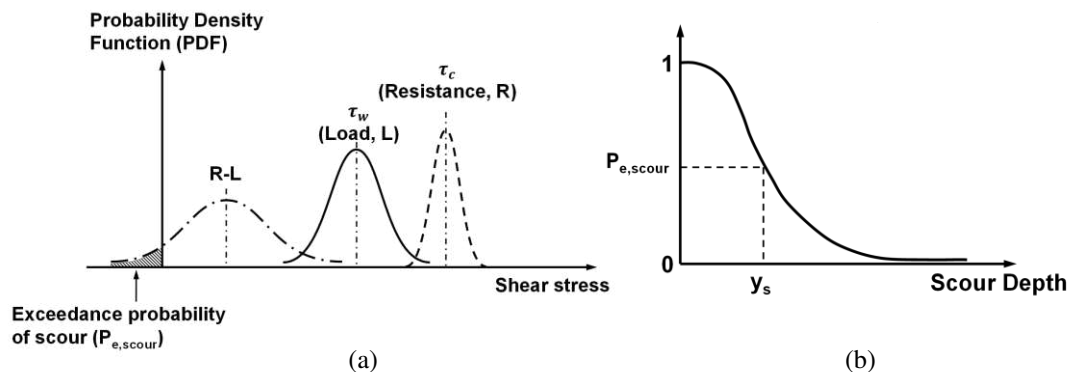

Figure 20. (a) Load distribution, resistance distribution, and exceedance probability of scour; (b) Exceedance probability vs. scour depth, Source: FHWA.

Uncertainty Consideration

Due to uncertainties related to flood occurrence, channel roughness estimates, and natural variability of field soils, the NextScour initiative also provided a probabilistic scour analysis that considered the variabilities of the water load and the soil resistance. The water load considers the following uncertainties:

- Natural uncertainties.

- Hydrological modeling uncertainties.

- Hydraulic modeling uncertainties.

- Equation uncertainty of the decay function.

The natural uncertainties consider the peak flood that a bridge experiences in its lifespan could have any return period, instead of only considering one design flood (e.g., Q_{100}). Hydrological modeling uncertainties include uncertainties in the parameters of the log-Pearson type III distribution. Hydraulic modeling uncertainties consider the uncertainty from the hydraulic models and the hydraulic input parameters. Here, only uncertainty of Manning's roughness n is included. Figure 18 illustrates the difference between the best-fit decay function and the actual CFD shear data points. The regression fitting results in equation uncertainty. Here, the bootstrapping method was used to generate the distribution of fitting both constants a and b in the decay function.

Probabilistic Scour Analysis

The Monte Carlo simulation (Doucet et al., 2001) was adopted for probabilistic scour analysis. It predicts the probability of a dependent variable by considering multiple independent variables as random variables following a certain distribution. The probabilistic scour analysis compared load to resistance, considering distributions of each. The distribution of the clay erosion resistance was obtained in the Clay Erosion Testing section. The load distribution (bed shear stress) started with generating annual maximum discharges with randomness for the entire bridge design life. Then hydraulic modeling converted these discharges to flow velocities and depths with uncertainty by considering Manning's roughness. Given the large number of Monte Carlo simulations needed, HEC-RAS was used to save computational time. The upstream approach bed shear stress (not affected by the bridge) was computed by using 1D flow velocity, hydraulic radius, and Manning's n. It was then amplified at the bridge by using the decay function when scour depth was zero. While the amplified shear stress at the bridge might vary from the CFD bed shear stress, a shear stress modification factor was applied to equalize both on the riverbed. Then the decay function determined how the shear stress would decay, along with the scour depth considering the equation uncertainty. The exceedance probability of scour at a given depth could be calculated when both load and resistance distribution were known, as plotted in Figure 20(b).

The probabilistic scour analysis was performed on the proposed new bridge by using a 10,000-point Monte Carlo simulation for a 75-year bridge design life. MDOT provided the HEC-RAS model for this project. It was a three-reach model with five discharge control cross sections. The HEC-RAS model was simplified to a one-reach model with one inlet upstream of the east channel. The U.S. Geological Survey gage 04157005 is about 20.1 km (12.5 mi) upstream of the Lafayette Avenue Bridge and does not represent the discharge at the bridge. When the annual maximum discharges are generated, the sample mean ($\bar{x}$), the sample standard deviation (σ_s), and the sample skewness (G_s) for the log-Pearson type III distribution were regressed by using the peak floods provided in the HEC-RAS model (Table 4), and the results are shown in Table 5. The R^2 value for the regression curves was 1.0, which indicated the regression was accurate. The regressed parameters were used to generate the population mean μ, population standard deviation σ, and population skewness G. N is the number of the annual peak discharges of the historical record, which was required when determining the distribution of μ, σ, and G. In this case, N was assumed to be 101, the total available annual records at gage 04157005.

Table 4. Peak-flood statistics from the HEC-RAS model.

Flow	Q_{10}	Q_{50}	Q_{100}	Q_{500}
Discharge (m³/s)	1,211.5	1,543.6	1,680.9	1,985.9

Table 5. Regressed sample parameters for log-Pearson Type III distribution.

Parameters	$\bar{x}$	σ_s	G_s
Value	2.898	0.146	−0.112

For the 10,000-points Monte Carlo simulation, 10,000 sets of μ_i, σ_i, and G_i ($i = 1, 2, \dots 10,000$) were generated. For each set of μ_i, σ_i, and G_i, 75 exceedance probabilities of floods ($P_{e,(i,j)}$, $j = 1, 2, \dots 75$) were randomly selected to represent the flow probability in each of the 75 years of bridge design life. In total, 750,000 discharges were generated. Figure 21 shows the probability mass function (PMF) of the 750,000 annual maximum discharge, and the PMF of the 10,000 maximum annual discharge every 75 years in the east channel.
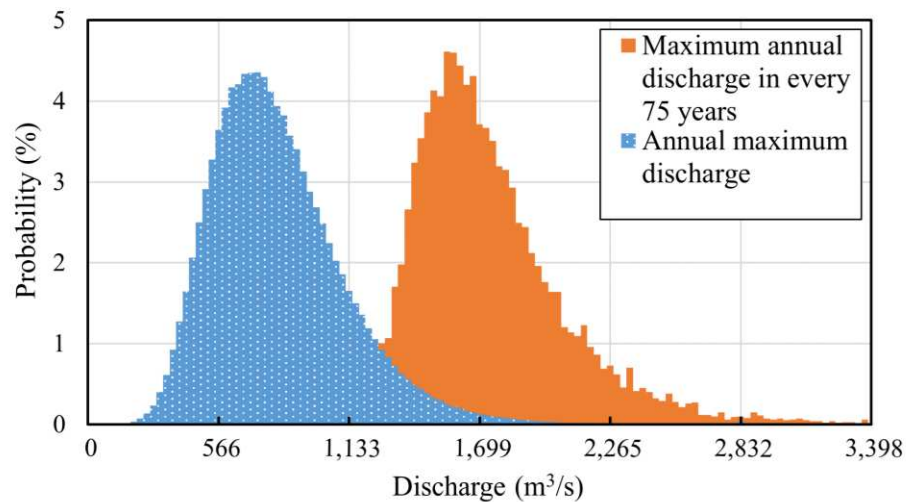

Figure 21. PMF of annual maximum discharge and maximum annual discharge in every 75 years for the Lafayette Avenue Bridge, Source: FHWA.

Table 6 compares the exceedance probability of various flood frequencies calculated from the generated data and the theoretical values. Generally, the exceedance probability of generated floods in 1 year was close to the theoretical values (which will lead to conservative results). Similarly, the exceedance probability for 75 years was also close to the theoretical value for generated floods of Q_{50} and Q_{100}. In contrast, the generated floods of Q_{200} and Q_{500} had a larger exceedance probability in 75 years than their theoretical values. This fact was due to the small number of N used in discharge generation. If N was larger, e.g., $N = 1,000$ or higher, the Monte Carlo simulation results and the theoretical value would be closer.

Table 6. Comparison of the exceedance probability: theoretical versus Monte Carlo.

Flood	Exceedance probability of flood frequency in 1 year (%)		Exceedance probability of flood frequency in 75 years (%)	
	Theoretical value	Monte Carlo	Theoretical value	Monte Carlo
Q_{50}	2	2.2	78	73.3
Q_{100}	1	1.2	52.9	52.3
Q_{200}	0.5	0.7	31.3	35.2
Q_{500}	0.2	0.3	13.9	19.9

In the HEC-RAS modeling, Manning's n is the only random variable considered. It is assumed to be constant and time-independent in the bridge design life. *NCHRP Report 761* (Lagasse et al., 2013) indicates that Manning's n follows a lognormal distribution with a COV of 0.015. Manning's n was 0.03 for the main channel and 0.08 for the overbanks in the revised HEC-RAS model. A total of 750,000 sets of discharges and 10,000 Manning's n were submitted to the revised HEC-RAS model via a batch job to compute the flow velocity and flow depth at the approach cross section. A total of 750,000 sets of bed shear stress for the total fender scour were calculated using the flow parameters obtained from HEC-RAS and Eq. 6 (HEC-18 Eq. 6.7; Arneson et al., 2012) as well as the best-fit decay function (Eq. 4).

$$\tau_a = \gamma R^{-\frac{1}{3}} \left(\frac{nV}{K_u}\right)^2 \tag{6}$$

Where γ is the specific weight of water, R is the hydraulic radius at the approach cross section, V is the velocity of the approach cross section, n is Manning's roughness coefficient, and K_u is 1.486 for English units and 1.0 for International System of Units (SI) units. CFD simulation more accurately captured the 3D flow pattern near the fender and the bridge piers. Therefore, it computed the actual bed shear stress near the fender on the riverbed. HEC-RAS calculated the approach bed shear stress using flow parameters of the approach cross section. The approach bed shear stress was amplified at the fender by using the amplification factor in the decay function, which may vary from the CFD bed shear stress at the fender. A shear stress modification factor, K_m, was applied to equalize both. Since a limited number of CFD simulations were run, the shear stress modification factors were correlated with the Froude number to provide a correlation function for all flow conditions. The correlation is expressed in the following equation:

$$K_m = 0.4\,Fr + 0.095 \tag{7}$$

Where F_r is the Froude number defined as $F_r = V/\sqrt{gR}$, and g is the acceleration of gravity.

Equation uncertainty of the best-fit decay function was determined using the bootstrapping method. A total of 20 out of 27 data points were randomly selected to fit the decay functions 50,000 times. The constants a and b in the decay function had a mean value of 7.14 and -0.81, respectively, agreeing with the coefficients in Eq. 4. The COVs of a and b were 0.03 and 0.13, respectively. Both constants were assumed to have a normal distribution.

CFD modeling of bed shear stresses at the fender and the piers already considered the contraction effect, so no separate contraction scour analysis was needed. Then the decayed shear stress was computed at 0.3-m (1-ft) incremental scour depths while applying the same shear stress modification factor. These shear stresses were compared with clay critical shear stress in the clay layer. The load distribution was the distribution of the 10,000 maximum bed shear stresses. Figure 22 shows the probability density function (PDF) of the bed shear stresses at selected scour elevations.
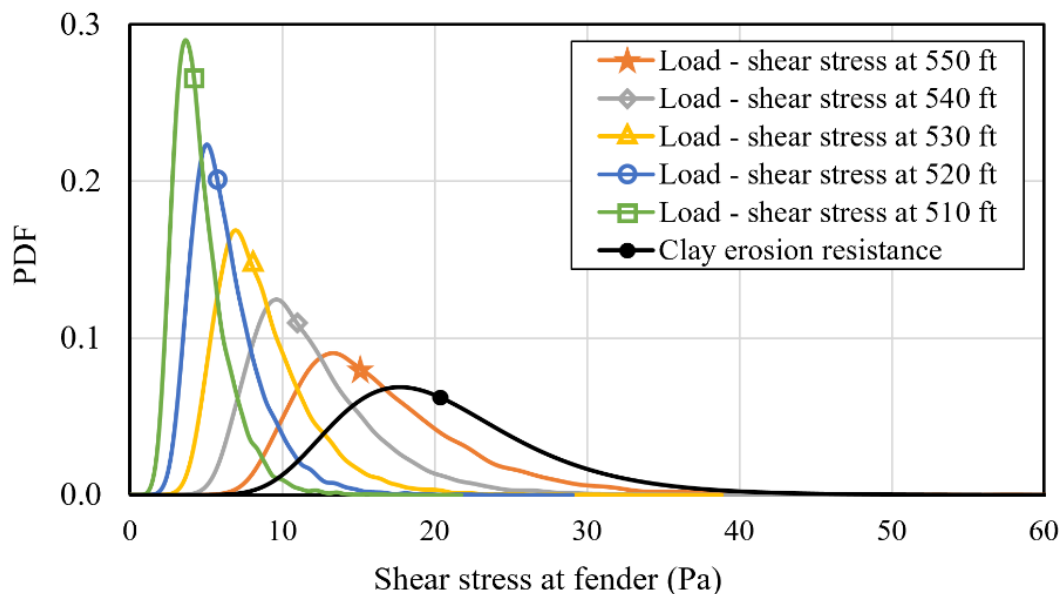

Figure 22. Bed shear stress distribution for total fender scour, Source: FHWA.

An assumption was made that the critical shear stress followed lognormal distribution, the parameters of which were calculated from the mean and COV of critical shear stress obtained in the Clay Erosion Testing section. The critical shear stress of the clay layer had a mean value of 20.5 Pa (0.43 psf) and a COV of 0.32 and followed the lognormal distribution. A total of 10,000 critical shear stresses were generated according to the obtained lognormal distribution. The clay erosion resistance curve in Figure 22 shows the PDF of the generated critical shear stresses. The load distribution of the total fender scour was compared against the resistance distribution. $P_{e,scour}$ was calculated as the probability of critical shear stress being less than the decayed bed shear stress at each target scour elevation. $P_{e,scour}$ values at each target scour depth are listed in Table 7, as well as shown in Figure 23.

Table 7. $P_{e,scour}$ of total pier scour at each scour elevation.

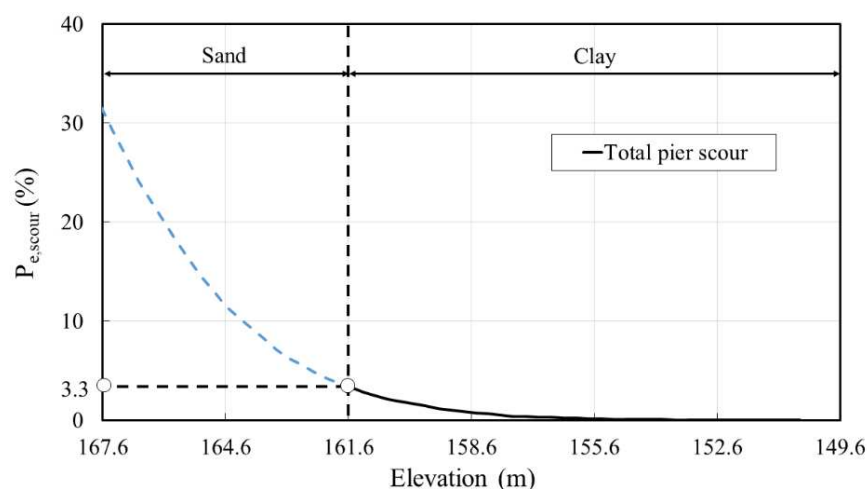| Scour elevation (m)	$P_{e,scour}$ for total pier scour (%)
167.6	31.6
164.6	11.5
161.5	3.3
158.5	0.7
155.4	0.2

Figure 23. Exceedance probability of the total fender scour at various elevations, Source: FHWA.

The probabilistic scour analysis assumed the clay started from the riverbed. In reality, the clay layer starts at the elevation of 161.5 m (550 ft). Therefore, the exceedance probability for elevations above 161.6 m (550 ft) was unreal and is represented as the dashed blue line in Figure 23. The probability of scour depth exceeding 161.6 m (550 ft) is 3.3 percent over 75 years of the bridge life span. Both deterministic and probabilistic scour analyses indicate that the clay layer would stop the scour. The result reduces the total scour from 12.5 m (41 ft) (Q_{500}) to 6.1 m (20 ft), a 51-percent reduction, which would reduce the H-pile sizes and the foundation design cost.

CONCLUSIONS

Through the TPF study, FHWA provided solid technical assistance to MDOT on the Lafayette Avenue Bridge replacement project. Hydraulic modeling using 3D CFD models found nominal shear stresses of 14.5 Pa (0.3 psf) for Q_{100} and 20.2 Pa (0.42 psf) for Q_{500} at the riverbed near the left upstream fender cylinder. The physical scour tests featured two 1:50 scale half-bridge models. Various approach velocities were used to observe the scour around fender cylinders, piers, and abutments. Scour tests revealed that the deepest scour happened upstream of the fender cylinders, and the abutment scour was minimal. CFD nominal bed shear stresses on incremental scour bathymetries, which were collected from the flume scour tests, were used to develop the decay functions of scour at the fenders. Soil erosion tests and the bootstrapping method identified that the critical shear stress of the clay below the 161.5-m (530-ft) elevation had a mean value of 20.5 Pa (0.43 psf) with a COV of 0.32.

A probabilistic scour analysis was conducted by using the Monte Carlo simulation. A total of 750,000 flow discharges were generated by considering various statistical uncertainties in the flood events. These discharges were modeled in a batch HEC-RAS considering a distribution of Manning's *n*. With the decay function equations and the computed approach shear stresses from the resulting Monte Carlo flow parameters, the distribution of decayed shear stress at 0.3-m (1-ft) incremental scour depth was calculated. The exceedance probability of the total fender scour for a continuous depth was determined by comparing the decayed shear stress against the soil resistance distribution at each depth. The exceedance probability of the total fender scour reaching the clay layer at 161.5 m (530 ft) was determined to be 3.3 percent in the 75-year bridge design life.

The 51-percent reduction of total scour demonstrated that NextScour could significantly improve the accuracy of bridge scour estimates. This study also provided MDOT with a tool to quantify the risk level of the bridge scour design.

ACKNOWLEDGMENTS

REFERENCES

Annandale, G.W. (2006). *Scour technology*, New York: McGraw-Hill.

Arneson, L., Zevenbergen, L., Lagasse, P., and Clopper, P. (2012). *Hydraulic Engineering Circular No. 18, Evaluating Scour at Bridges, 5th ed.,* Report No. FHWA-HIF-12-003, Washington, DC: Federal Highway Administration.

Briaud, J.L., Chen, H.C., Chang, K.A., Oh, S.J., Chen, S., Wang, J., Li, Y., Kwak, K., Nartjaho, P., Gudaralli, R., Wei, W., Pergu, S., Cao, Y.W., and Ting, F. (2011). *The Sricos – EFA Method Summary Report*, Texas A&M University.

Doucet, A., Freitas, N., and Gordon, N. (2001). "Sequential Monte Carlo methods in practice", *Statistics for Engineering and Information Science*, New York: Springer.

Federal Highway Administration. (2020). "TPF-5(461) Soil and Erosion Testing Services for Bridge Scour Evaluations." <https://www.pooledfund.org/Details/Study/688> (Jan. 5, 2022).

Guo, J., Suaznabar, O., Shan, H., and Shen, J. (2012). *Pier Scour in Clear-Water Conditions with Non-Uniform Bed Materials*, Report No. FHWA-HRT-12-022, Washington, DC: Federal Highway Administration.

Lagasse, P. F., Ghosn, M., Johnson, P. A., Zevenbergen, L. W., and Clopper, P. E. (2013). *Reference Guide for Applying Risk and Reliability-Based Approaches for Bridge Scour Prediction*, NCHRP Report 761, Washington, DC: Transportation Research Board.

FHWA (2021). "LTBP InfoBridge, Lafayette Avenue Bridge Information." <https://infobridge.fhwa.dot.gov/Data/BridgeDetail/23628903>, (May 18, 2022).

Shan, H., Kilgore, R., Shen, J., and Kerenyi, K. (2016). *Updating HEC-18 pier scour equations for noncohesive soils*, Report No. FHWA-HRT-16-045, Washington, DC: Federal Highway Administration.

Shan H, Pagenkopf, J., Kerenyi, K., and Huang, C. (2021a). "NextScour for improving bridge scour design in the United States." *Proc. of the Institution of Civil Engineers - Forensic Engineering*, 173(4), 121–129.

Shan, H., Shen, J., Kilgore, R., and Kerenyi, K. (2015). *Scour in cohesive soils*, Report No. FHWA-HRT-15-033, Washington, DC: Federal Highway Administration.

Shan, H., Wagner, A., Kerenyi, K., Guo, J., and Xie, Z. (2011). "An ex-situ scour testing device for erosion research of cohesive soils." *Proc. 2011 Engineering Mechanics Institute Conference*, Boston, Mass., 1020–1027.

Shan, H., Wiblishauser, O., Kerenyi, K., Shen, J., Meyer, T., Pastrich, D., Pagenkopf, J., and Tsou, N. (2018). "An in situ scour testing device for determining soil erosion resistance." *Proc. of the 9th International Conference on Scour and Erosion*, Taipei, Taiwan, 559–566.

Shan H., Wiblishauser, O., Kerenyi, K., Uhrig, M., Huang, C., and Pagenkopf, J. (2021b). "Efficient automated laboratory testing of erosion resistance for fine-grained soils." *Proc. of the 10th International Conference on Scour and Erosion*, Arlington, VA, 1063–1071.

Stine R. (1989). "An Introduction to Bootstrap Methods: Examples and Ideas." *Sociological Methods & Research*, 18(2-3),243-291.

URS. (2014). *Feasibility study of bridge repair and replacement alternatives – Lafayette Avenue (M-13/M-84) over the east channel of the Saginaw River*. Grand Rapids, MI: URS Corporation.

Zinner, M., Meyer, T., Shan, H., Shen, J., Kerenyi, K., and Bergendahl, B. (2016). "A field erodibility testing device for scour evaluation of bridges." *Proc. of the 8th International Conference on Scour and Erosion,* London, UK, 1107–1114.

INTERNATIONAL JOURNAL OF GEOENGINEERING CASE HISTORIES